LUND UNIVERSITY

Bandwidth enhancement technique for broadside tri-modal patch antenna

Chiu, Chi-Yuk; Lau, Buon Kiong; Murch, Ross

Bandwidth Enhancement Technique for Broadside Tri-Modal Patch Antenna

Chi-Yuk Chiu, *Senior Member, IEEE*, Buon Kiong Lau, *Senior Member, IEEE* and Ross Murch, *Fellow, IEEE*

Abstract—A technique for enhancing the bandwidth of a broadside tri-modal patch antenna is described. The key idea of the technique is to incorporate a dual-resonance structure into the broadside tri-modal patch geometry. By increasing one edge of the tri-modal patch while decreasing its size at the opposite edge, the resulting structure can be viewed as two super-imposed Y-shaped structures of different resonant frequencies. This intuition is confirmed using characteristic mode analysis (CMA). Furthermore, guided by CMA, further modifications enable two sets of resonant modes to be tuned for increasing the bandwidth of the tri-modal patch antenna. Importantly, the proposed bandwidth enhancement technique does not affect the desired broadside radiation patterns significantly. Therefore, it can be utilized to modify the tri-modal patch antenna without degrading its potential for massive MIMO array application. Measurement results show that the technique enhances the 10 dB impedance bandwidth from 4.3% to 19.7% with the largest antenna dimension of $0.48\lambda_c$, where λ_c is the wavelength in air at the center frequency. The design example of the proposed technique is able to cover widely used 3 GHz bands in 5G communication systems and its potential usage in massive MIMO arrays is demonstrated.

Index Terms—Broadside radiation, characteristic modes, multiport antenna, multiple-input multiple-output (MIMO) array.

I. INTRODUCTION

ONE challenge of 5G and other advanced wireless communication systems is to meet the requirement of multigigabit throughput. One approach to meeting this challenge is to use massive multiple-input multiple-output (MIMO) systems [1], [2], in which multiple users can be served simultaneously and individual user throughputs are considerably enhanced. However, when the number of antenna ports in a massive MIMO system corresponds to hundreds or more, the overall antenna size becomes a critical consideration. The antenna size may not be a serious problem for millimeter-wave systems, but it can be a hurdle for the development of massive MIMO systems in the sub-6 GHz spectrum. Furthermore, today's massive MIMO arrays typically consist of dual-port, dual-polarized broadside antennas as unit cells, to provide

Chi-Yuk Chiu is with the Department of Electronic and Computer Engineering, The Hong Kong University of Science and Technology, Clear Water Bay, Kowloon, Hong Kong (e-mail: eefrankie@ust.hk).
Buon Kiong Lau is with the Department of Electrical and Information Technology, Lund University, SE-221 00 Lund, Sweden (e-mail: buon_kiong.lau@eit.lth.se).
Ross Murch is with the Department of Electronic and Computer Engineering and the Institute for Advanced Study, The Hong Kong University of Science and Technology, Clear Water Bay, Kowloon, Hong Kong (e-mail: eermurch@ust.hk).

outdoor base stations with uniform sectorized coverage. These unit cells must also be spaced sufficiently apart to ensure low mutual coupling and correlation, which are important for efficient massive MIMO operation.

Recently, two tri-port broadside antenna elements suitable for conventional mobile frequency bands (sub-6 GHz) have been proposed [3]-[5]. These elements can be used as unit cells to realize more compact massive MIMO arrays for outdoor base stations, since they contain more than two ports per element. In [4], a multipolarized wideband circular patch antenna proposed for MIMO operation is shown to provide three 120°-displaced linearly polarized waves by exciting the fundamental (TM_{11}) mode using three probe feeds. Furthermore, the tri-port circular patch, printed on an FR-4 epoxy board, is originally envisioned for standalone use in on-wall access point applications [4], where the 30° tilts observed in its broadside patterns is not a critical issue. In another approach, that was inspired by a two-port Y-shaped patch antenna [6], a regular broadside snowflake-shaped patch, with 6th order rotational symmetry, was developed for exciting three modes simultaneously with different weightings in a tri-modal manner [5]. Using insights from characteristic mode analysis (CMA) [7], [8], it was discovered that the first two modal patterns with broadside radiation were equally shared by three antenna ports. To achieve low pattern correlation, a third mode of a non-broadside pattern was also excited by the three ports. The all-metal design has high power capability, and since it requires no substrate material, it does not depend on tolerances of the substrate materials. Other multi-mode patch antenna designs [9]-[12] do not provide patterns that are all in the broadside direction. These designs are more suitable for indoor MIMO applications where the exact antenna pattern shape is less critical for coverage due to the rich multipath propagation in indoor environments. More explicit comparisons of recent tri-port designs are also provided in Table I. Although the tri-modal broadside snowflake-shaped patch antenna [5], with 6th order rotational symmetry, has provided a new approach for designing compact massive MIMO arrays, the measured 4.3% impedance bandwidth needs to be improved to cope with practical needs.

To extend the bandwidth of the broadside tri-modal patch antenna, we propose a bandwidth enhancement technique which is particularly suitable for antenna structures with metal components. The key idea of the bandwidth enhancement technique is to create a dual-resonance structure, from the tri-modal patch structure, by dividing it into two Y-shaped patches. This is achieved by increasing the size of one edge of the patch while decreasing its size at the opposite edge,

TABLE I
COMPARISON OF RECENT TRI-PORT MIMO ANTENNAS

Tri-port antennas	[4]	[9]	This work
Operating mechanism	Three 120°-displaced linearly polarized broadside waves generated by exciting fundamental (TM$_{11}$) mode using three probe feeds	Three wideband monopolar patch antennas generating monopole-like waves integrated into a Y-shaped structure	Each of the three ports excites 2 sets of 3 modes in different weightings to produce wideband dual resonances. The broadside patterns of each of the ports have the same coverage but remain orthogonal due to the different mode weightings
Patch material	Copper and FR-4	Copper and FR-4	Copper only
Electrical size (λ_c)*	$0.63\lambda_c \times 0.63\lambda_c \times 0.13\lambda_c$ (Patch printed on FR-4 substrate)	$0.66\lambda_c \times 0.57\lambda_c \times 0.13\lambda_c$ (Patch printed on FR-4 substrate)	$0.48\lambda_c \times 0.48\lambda_c \times 0.11\lambda_c$ (Patch in the air)
Reported bandwidth	24%	24%	19.7%
Measured minimum isolation (dB)	14	14.5	14.3
Minimum ECC	0.05	Much less than 0.1	0.02
Measured peak gain (dBi)†	6.6 (with square ground plane: 150 mm × 150 mm)	N/A (with circular ground plane: diameter of 150 mm)	7.5 (with circular ground plane: diameter of 100 mm)
Measured peak efficiency	96%	92%	92%
Antenna array study	No	No	Yes

* λ_c is the wavelength in air at the center frequency.
† Measured peak gain is the product of measured total efficiency and directivity.

allowing the structure to function as two connected Y-shaped patches [6]) with two slightly different resonant frequencies. As confirmed by CMA, this modification offers two sets of resonant modes that can be used to increase the bandwidth of the patch antenna, while retaining broadside patterns and low pattern correlation across the three ports. The advantage of this approach is that it does not require slots [13], [14] or additional parasitic elements [15], [16]. Moreover, both the slot and parasitic element approaches were found to be unsuitable for the tri-modal patch antenna since it was not clear how these techniques can create another set of three resonant modes for the excitation of three orthogonal broadside patterns by three antenna ports. Furthermore, the proposed technique does not significantly affect the radiation patterns over the wider bandwidth. Specifically, broadside radiation patterns can be retained over a relatively wide frequency band, such that the bandwidth enhanced tri-modal patch antenna is even more suitable for compact massive MIMO array implementation in outdoor scenarios [5]. Intuitively, similar broadside patterns

are supported over the wide bandwidth since each of the two resonances can be attributed to the same basic Y-shaped design.

The proposed technique also has the additional benefit that it has 120° or 3rd order rotational symmetry, such that the coupling between adjacent elements can be more balanced than that for conventional dual-polarized square patch elements. This feature facilitates a smaller inter-element spacing for a given coupling level, and hence a more compact array configuration than the square patch even for the wideband design.

Previous efforts in applying CMA for bandwidth enhancement largely focused on the merging of new resonant modes created by adding physical features (e.g., metal strips and bezel [17], [18]), rather than modifying the existing structures in the way proposed in this work. Moreover, preserving the antenna pattern within the operating band had not been a consideration.

The primary contribution of this work is the systematic development of a bandwidth enhancing technique suitable for

a broadside tri-modal antenna. CMA plays a critical role in enabling the design process through providing insights on structural dependent modes as well as feeding strategies. In addition, full-wave simulation and measurement results are provided to validate the effectiveness of the approach.

This paper is organized as follows. In Section II, a bandwidth enhancement technique suitable for tri-modal patches [5], is proposed. In Section III, possible feed regions are determined and matching is discussed, based on their corresponding electric field distributions and feed structuring. Section IV shows that the design achieves 19.7% in measured bandwidth without using any lumped element for matching. The corresponding radiation performance is also presented and evaluated. In Section V, results are provided when seven of the proposed wideband tri-broadside radiation antennas are concatenated together. The design examples included cover the widely used 3 GHz bands in 5G communication systems and their potential usage in massive MIMO arrays is demonstrated. Finally, conclusions are drawn in Section VI.

II. Modified Tri-Modal Patch and Modal Analysis

To overcome the narrowband performance of the tri-modal patch antenna [5], a bandwidth enhancement technique is introduced in this section. The geometry considered is shown in Fig. 1 and consists of a metal regular snowflake-shaped patch radiator suspended in air with six identical branches that exhibits 6th order rotational symmetry. All the branches are folded downward towards, but do not touch, a ground plane underneath. A hexagonal capacitive loading plate with three shorting pins is added between the radiator and ground plane. Three feeding probes were also attached to the plate to provide excitation. The overall antenna structure, including the hexagonal loading plate, exhibits 120° or 3rd order rotational symmetry when viewed from the top. The tri-modal patch evolved from a dual-port Y-shaped patch [6] and CMA analysis of that patch showed that, apart from two resonant broadside modes within the frequency range of interest, a

third mode is near-resonant. By adding the capacitive loading plate and 3 more branches to the Y-shaped patch, the third mode was successfully tuned to resonance, hence providing the possibility to create three uncorrelated ports from the modified patch structure. Furthermore, to excite the three modes jointly and in an orthogonal way, characteristic electric field distributions from CMA were used to find the feed positions. Although the tri-modal broadside snowflake-shaped patch antenna has provided a new way to design a compact unit cell for massive MIMO arrays, the measured 4.3% impedance bandwidth needs to be further improved to meet practical needs.

To increase the bandwidth of the tri-modal antenna, a new bandwidth enhancing technique is developed to retain the same broadside radiation patterns over the frequency band. The technique is based on creating a dual-resonance structure from the underlying dual Y-shaped design [6]. In particular, the original Y-shaped design was shown to provide two resonant broadside modes by itself [5]. Therefore, the merging of two Y-shaped patches has the potential to not only enhance a third mode into resonance [5], but also to provide dual resonances if the two Y-patches are dimensioned differently. In other words, the existing snowflake structure was modified to achieve different electrical sizes of the two constituting Y-shaped patches, so to opportunistically obtain dual-resonances of the two desired broadside modes. At the same time, using two different Y-shaped patches to make a snowflake should still support an additional mode (or modes) with radially outward currents. This hypothesis was tested and indeed, there are six modes that can be utilized for designing a wideband
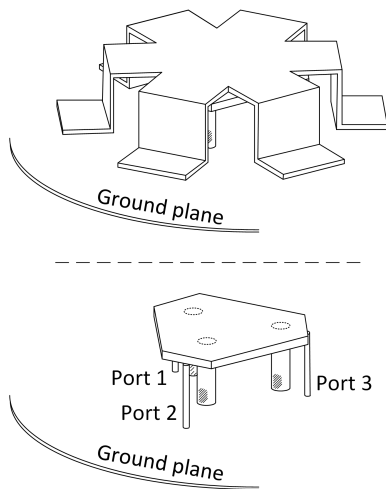

Fig. 1. Geometry of tri-broadside radiation antenna: (top) regular snowflake-shaped patch antenna; (bottom) hexagonal capacitive loading plate with three shorting pins.
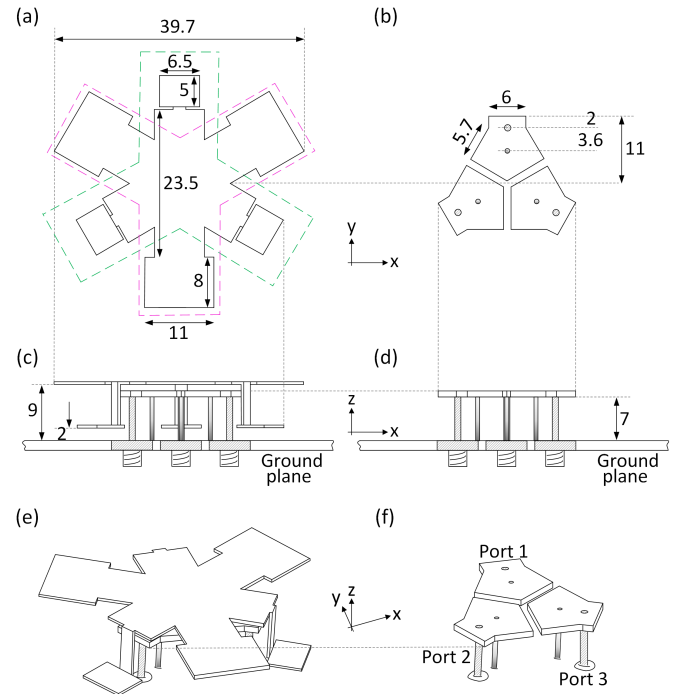

Fig. 2. Geometry of proposed wideband tri-broadside radiation antenna (units: mm): (a) plan view; (b) plan view without radiator; (c) side view; (d) side view without radiator; (e) perspective view; and (f) perspective view without radiator.

tri-modal antenna. The result of applying this technique to the tri-modal antenna element is shown in Fig. 2 where key dimensions of the structure are also provided. The original six identical branches are changed into two overlapping Y-structures and interlaced with each other as shown in Fig. 2(a) with the purple and green dashed lines encircling them. In this new snowflake configuration, only half of the branches are folded downward towards the ground plane, and their sizes are reduced. The other half are left unfolded and enlarged at the end. As expected, this new snowflake patch structure offers six resonant modes in the frequency band of interest, as can be seen in Fig. 3(a). The eigenvalues were calculated from the electromagnetic simulation software Altair FEKO [19] independently of the antenna feed location. The eigenvalues are numbered by the order of their zero-crossing. Infinite ground was assumed in the FEKO CMA simulation to avoid dealing with many finite-ground based CMs, which will complicate CMA. Furthermore, to verify that modal tracking was correctly performed by FEKO over the relatively large frequency range, the characteristic far-fields were carefully checked to ensure no abrupt pattern change in frequency. This is because the far-fields have been found to be relatively stable in frequency [20]. No erroneous tracking was detected. In Fig. 3(a), Modes 1-3 are mainly attributed to the unfolded Y-shaped part, whereas the folded Y-shaped part contributes to Modes 4-6. However, with this modification, the two groups of modes are still too far away from each other to achieve a dual-resonance band. In particular, the zero-crossing eigenvalues of Modes 2 and 3, and Modes 4 and 5 occur around 2.8 GHz and 3.8 GHz, respectively.

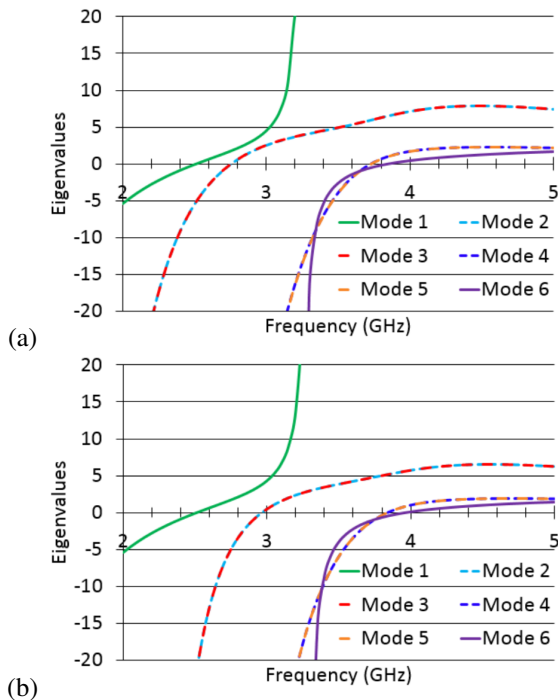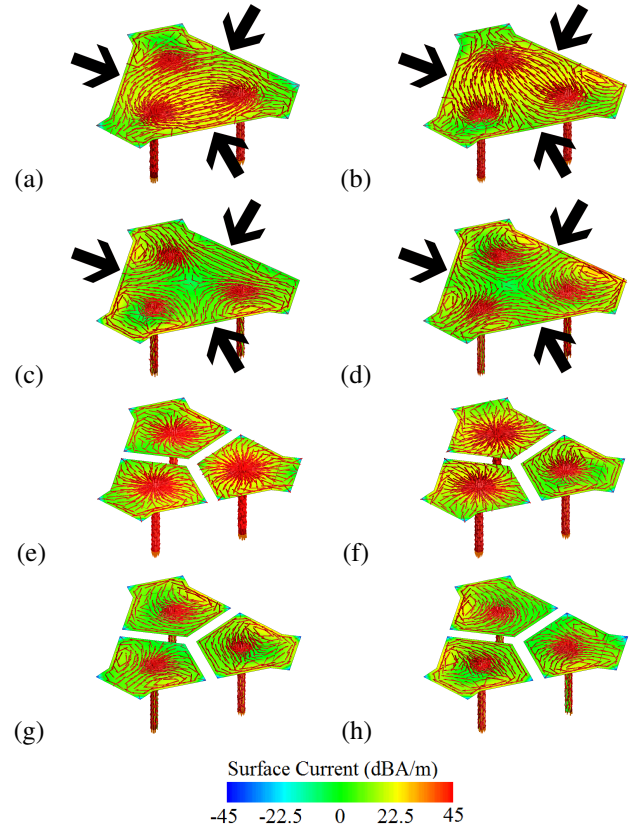To overcome this problem, it was observed in Fig. 4(a)-

Fig. 4. Modal current distribution on capacitive loading plates: (Union version) Modes 2 and 3 at 2.8 GHz correspond to (a) and (b); (Union version) Modes 4 and 5 at 3.8 GHz correspond to (c) and (d); (Split verson) Modes 2 and 3 at 3.0 GHz correspond to (e) and (f); (Split verson) Modes 4 and 5 at 3.8 GHz correspond to (g) and (h).

Fig. 3. Eigenvalues of first six characteristic modes with (a) union and (b) split capacitive loading plates.

(d) that the currents of Modes 2 and 3 flow across the entire hexagonal plate, whereas those of Modes 4 and 5 do not. Therefore, to shorten the resonant paths of Modes 2 and 3 without significantly affecting Modes 4 and 5, the single loading plate of the original design (see Fig. 1) was split into three parts, as shown in Fig. 2(b). Each plate is now attached with one shorting pin and one feeding probe, and the overall structure retains the feature of 120° or 3rd order rotational symmetry. This observation is consistent with the effect of splitting modal current distributions, as can be seen in Fig. 4(e)-(h). The currents of Modes 4 and 5 are largely the same as before the splitting, unlike those of Modes 2 and 3.

As can be seen in Fig. 3(b), the splitting of the plate closes the frequency gap between the two groups of modes, as it increases Modes 2 and 3's resonant frequencies to around 3 GHz, while keeping those of Modes 4 and 5 almost constant (~3.8 GHz).

Compared to [5], the proposed modifications to the antenna structure have introduced three additional resonant modes close to the original three modes. This forms the basis to widen the impedance bandwidth by merging nearby resonances. However, this consideration alone is inadequate because it does not guarantee that the desired broadside radiation can be maintained over the large bandwidth. Therefore, the far-field patterns of the six resonant modes from 3.0 GHz to 4.0 GHz as
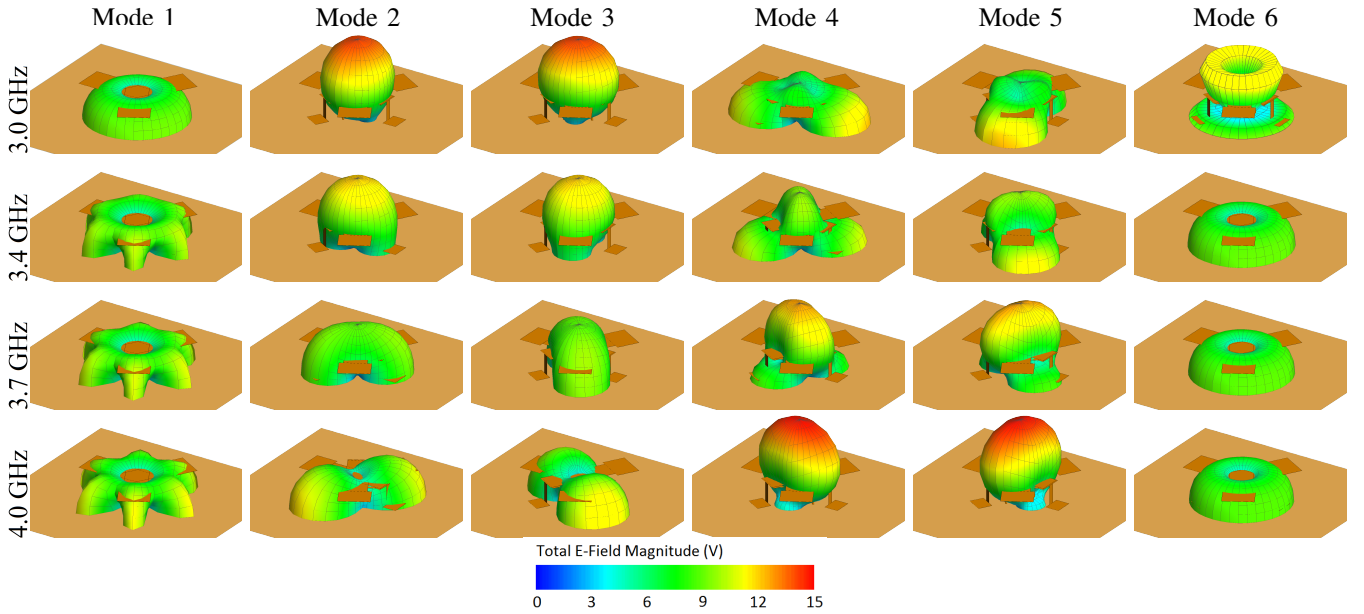
Fig. 5. Modal far-field patterns of modified snowflake-shaped patch with split capacitive loading plates.

shown in Fig. 5 were further investigated. As can be seen, the evolved structure inherits the radiation pattern characteristics of a regular snowflake-shaped plate at 3.0 GHz. Two modes exhibit broadside radiation and one mode has a monopole-like pattern. These three modal far-field patterns have been verified to support three ports with broadside radiation patterns with low mutual coupling [5]. At 3.4 GHz, although the monopole-like pattern is slightly distorted, the general shape is still maintained. At 3.7 GHz, the patterns of Modes 1 to 3 become less broadside. On the other hand, Modes 4 and 5 start to exhibit broadside radiation and Mode 6 offers a monopole-like pattern. At 4.0 GHz, Modes 4 to 6 take up the role for generating tri-port broadside patterns whereas the contributions from Modes 1 to 3 are diminished. It is noted that the assumption of infinite ground in the FEKO simulation has resulted in the maximum field intensity to be on the xy-plane for certain modes and frequencies (e.g., Mode 1). This is because the image theory applies, as in the case of an ideal quarter-wave monopole on an infinite ground plane.

III. FEED DESIGN

To determine the appropriate probe feed locations, a similar procedure as proposed in [5] is adopted, except that in this paper, the chosen feed should excite the electric near-fields of two sets of modes to obtain dual resonance across the three ports (rather than only dealing with a single set of three modes). To begin with, the z-directed ports should be located where the fields are strong for all three modes, to excite them simultaneously. As in [5], the amplitude of the characteristic E-field distributions (0.5 mm below the modified top patch) points to suitable regions being along the three folded branches close to the folded edges. Then, the phase distributions of z-directed characteristic E-fields are as illustrated in Fig. 6. To excite a tri-port broadside antenna with orthogonal radiation patterns, there should be a nearly 180° phase shift between

the excitation of two broadside modes (i.e. Modes 2 and 3 at 3.0 GHz or Modes 4 and 5 at 4.0 GHz) by the different ports [5]. Based on this requirement, the possible regions for the three feeding ports to excite both resonant frequencies are indicated by the red, green and blue boxes in Fig. 6. Note that the possible regions are larger if only the first resonance is considered, which is in line with the result presented in [5]. As can be seen, the possible feeding port locations are now confined to the central line of each small capacitive loading plate extending from the shorting pin to the perpendicular edge. By sliding the antenna probe along the line, a change in impedance matching for the dual-resonance excitation can be observed. In this context, the optimum probe feeding location for dual-resonance excitation was found to be 2 mm away from the outer edge of each small capacitive loading plate. With the analysis of eigenvalues, characteristic far-field patterns and port locations, it is expected that the proposed evolved snowflake-shaped structure can provide two nearby resonances and support three broadside patterns with low correlation.

It should be noted that, apart from increasing the resonant frequencies of Modes 2 and 3 (to create a dual-resonance band), the splitting of the capacitive loading plate connected to three feeding probes into three equal parts also helps in facilitating wideband impedance matching. From Fig. 7, it can be observed that the input impedance locus of the single capacitive loading plate (union plate) is on the right lower quadrant of the Smith chart at the higher frequencies. By splitting the loading plate into three pieces, shunt capacitances are created between the plates and the original series capacitance is reduced. The additional shunt capacitances cause the admittance to be rotated in a clockwise direction. Moreover, the impedance is rotated in a clockwise direction due to the smaller series capacitance (which resemble adding a series inductance for reactance compensation). Consequently, the input impedance locus of the split plates at the higher frequencies
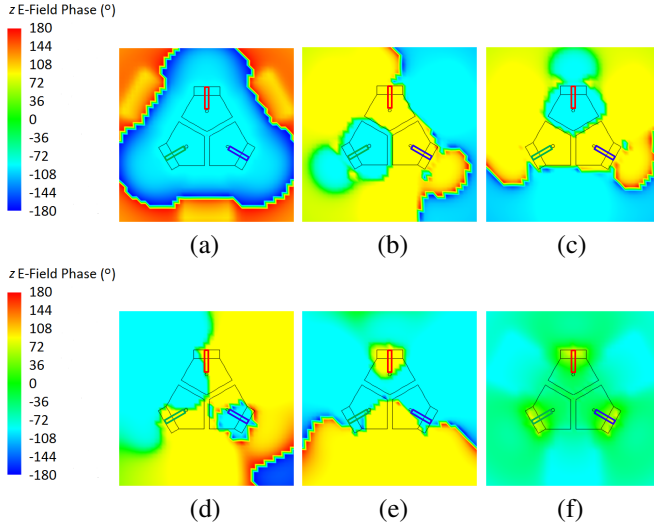
Fig. 6. Phase distribution of z-directed characteristic E-fields at 0.5 mm below the top snowflake patch: Modes 1–3 at 3.0 GHz correspond to (a)–(c); Modes 4–6 at 4.0 GHz correspond to (d)–(f).

Fig. 8. Prototype of wideband tri-port broadside antenna.
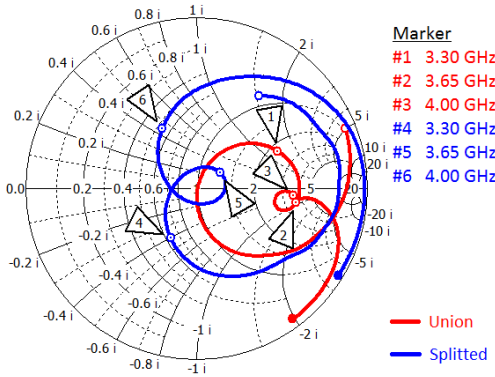

Fig. 7. Simulated input impedance at port 1 with union and split capacitive loading plates.

is now located near the center of the chart. More importantly, the input impedance locus at the lower frequencies can also be kept close to the center, which means that the impedance matching effect is favorable for both resonances.

IV. ANTENNA PERFORMANCE

In this section, the actual performance of the bandwidth enhanced tri-port broadside antenna is evaluated by both full-wave simulation and measurement. The simulation results were calculated using the time-domain solver CST Microwave Studio (2019 version) [21]. For measurement, a prototype was fabricated, as shown in Fig. 8. The evolved snowflake-shaped radiator on the top and the three capacitive loading plates inside are made of 0.5 and 1 mm-thick copper sheets, respectively. The three shorting pins are made of 0.7 mm-diameter copper rods. To ensure the three antenna ports exhibit similar performance, the entire upper structure was mounted on a circular ground plane with the diameter of 100 mm. For convenience, instead of a copper plate, the ground plane is made on a FR-4 epoxy board with thickness of 1.6 mm, cut into a circular shape, with a copper layer on each side of the
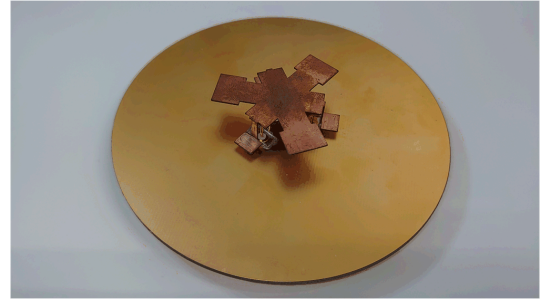
substrate. Three rectangular openings were made on the board for integrating the SubMiniature version A (SMA) connectors.

From Fig. 9(a), it is observed that all three antenna ports exhibit identical impedance matching characteristics in simulation, due to the perfect 120° rotational symmetry of the antenna structure. For the same reason of symmetry, some coupling coefficients are redundant and hence omitted for simplicity. The 10 dB impedance bandwidth of each antenna port is from 3.30 GHz to 3.97 GHz (i.e.,18.4%). The relatively large bandwidth is formed because of the merging of two nearby resonances at 3.51 GHz and 3.86 GHz. Compared to the results of CMA in Section II, the insertion of the feeding probes has further adjusted the first resonance to a higher frequency, which assists in obtaining a dual-resonance band. The isolation between any two ports is between 14.3 dB to 47.2 dB within the operating bandwidth. The simulation S-parameters show good agreement with the measurements. Port 1 of the fabricated prototype has a 10 dB bandwidth from 3.25 GHz to 3.96 GHz (i.e., 19.7%) as illustrated in Fig. 9(b). Due to the fabrication tolerances of the handmade structure, it is difficult to obtain identical performance from the three antenna ports as in simulation. However, the matching and mutual coupling performance for all ports are still very close to one another. Furthermore, the measurement results also verify the wideband operation of the evolved snowflake-shaped patch antenna.

Figure 9(c) shows both the simulated and measured antenna efficiencies and gains of port 1. Again, in the ideal case (i.e., full-wave simulation) with a circular ground plane, the three ports achieve the same performance. The discrepancy between the simulated and measured results as seen in the figure can be mainly accounted for by the soldering metal used in the fabricated prototype. Nevertheless, the prototype provides measured efficiency of 73% to 92% over the operating bandwidth with a measured peak gain of 7.5 dBi. It should be pointed out that the proposed antenna structure has the potential to attain wider impedance bandwidth according to CMA results (by keeping the two sets of resonant modes further apart), but such designs will be subject to larger variations of efficiency and gain around the middle of the operating frequency band. For example, when the gaps among the three split capacitive loading plates are all reduced by 0.8 mm, the simulated bandwidth can be increased to 22%. In addition to the bandwidth, efficiency and gain, the achieved radiation patterns also need to be studied. The simulated and
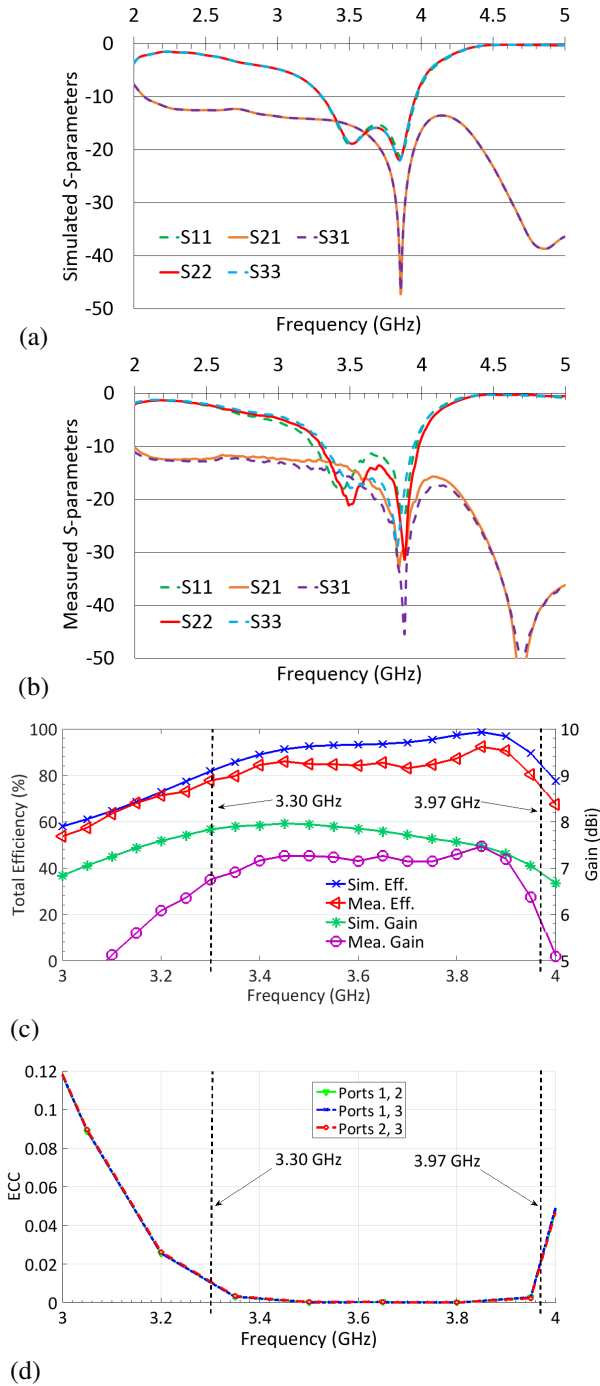
Fig. 9. Performances of proposed wideband tri-broadside radiation antenna: (a) simulated S-parameters; (b) measured S-parameters; (c) simulated and measured efficiencies and gains of port 1; and (d) envelope correlation coefficients calculated from simulated far field patterns.

Fig. 10. Radiation patterns of proposed wideband tri-port broadside antenna obtained at port 1 with simulation (solid), measurement (dash-dot), E-phi (red), and E-theta (blue).

field patterns near their respective resonant frequencies. The envelope correlation coefficients (ECCs) between any two ports within the frequency band of interest, as calculated from the far field patterns, is below 0.02 as depicted in Fig. 9(d). Due to symmetry, the simulated ECC curve between any two ports is identical.

V. ANTENNA ARRAY AND DISCUSSION

One key advantage of developing a compact tri-port broadside antenna with low correlation is that it may be used as a unit cell for a massive MIMO array. The Ergodic sum rate of a 102-port array built by tessellating 34 tri-port (tri-modal) broadside antennas was evaluated in [5]. It was shown that the sum rate performance of utilizing the relatively narrowband broadside antenna array is close to that achieved by using an ideal antenna array, with only a 1-2 dB gap. Since the bandwidth enhancement technique used in this work does not affect the 120° rotational symmetry of the base design in [5], the resulting wideband antenna can also be used to build a massive MIMO array in the same manner as in [5].

Figure 11(a) illustrates seven proposed wideband tri-port radiation antennas tessellated over a flat surface (21-port array). For integration into an array configuration, the circular ground plane of each unit cell was modified into a hexagonal shape with the edge length of 34.6 mm (retaining the 120° rotational symmetry). All the ground planes were connected together to be a common ground. The remaining parameters were kept unchanged as those given in Section II. Such an antenna array can be extended to contain any number of unit

measured radiation patterns at port 1 at 3.4 GHz, 3.6 GHz and 3.8 GHz are plotted in Fig. 10. It is observed that all the cuts with x-axis are pointing at the broadside direction, as desired. Note that the E-phi patterns in the simulated yz-planes are too small in magnitude to be shown in the figure. The broadside radiation characteristic occurs over the wide frequency band because the two antenna resonances come from two groups of resonant modes (Modes 1 to 3 and Modes 4 to 6 described in Section II), in which they have similar characteristic far-
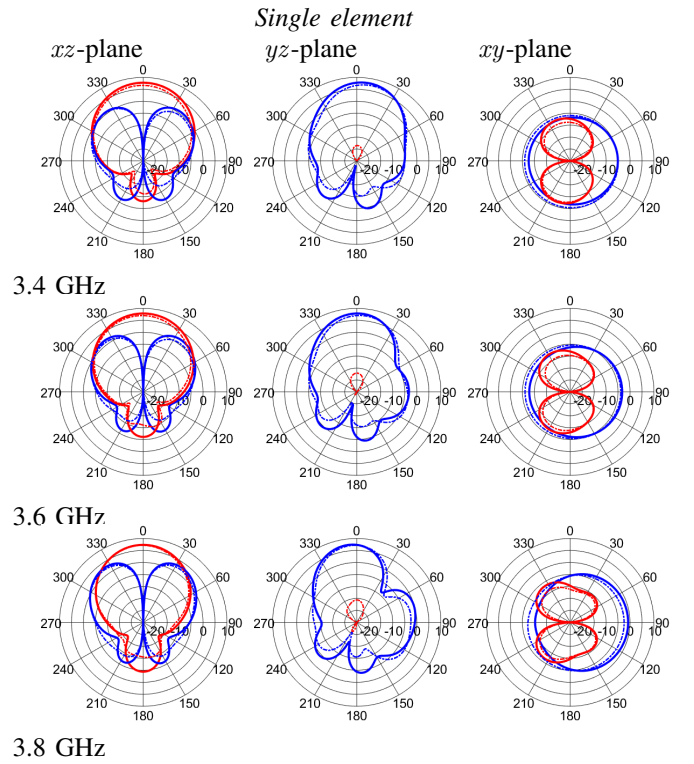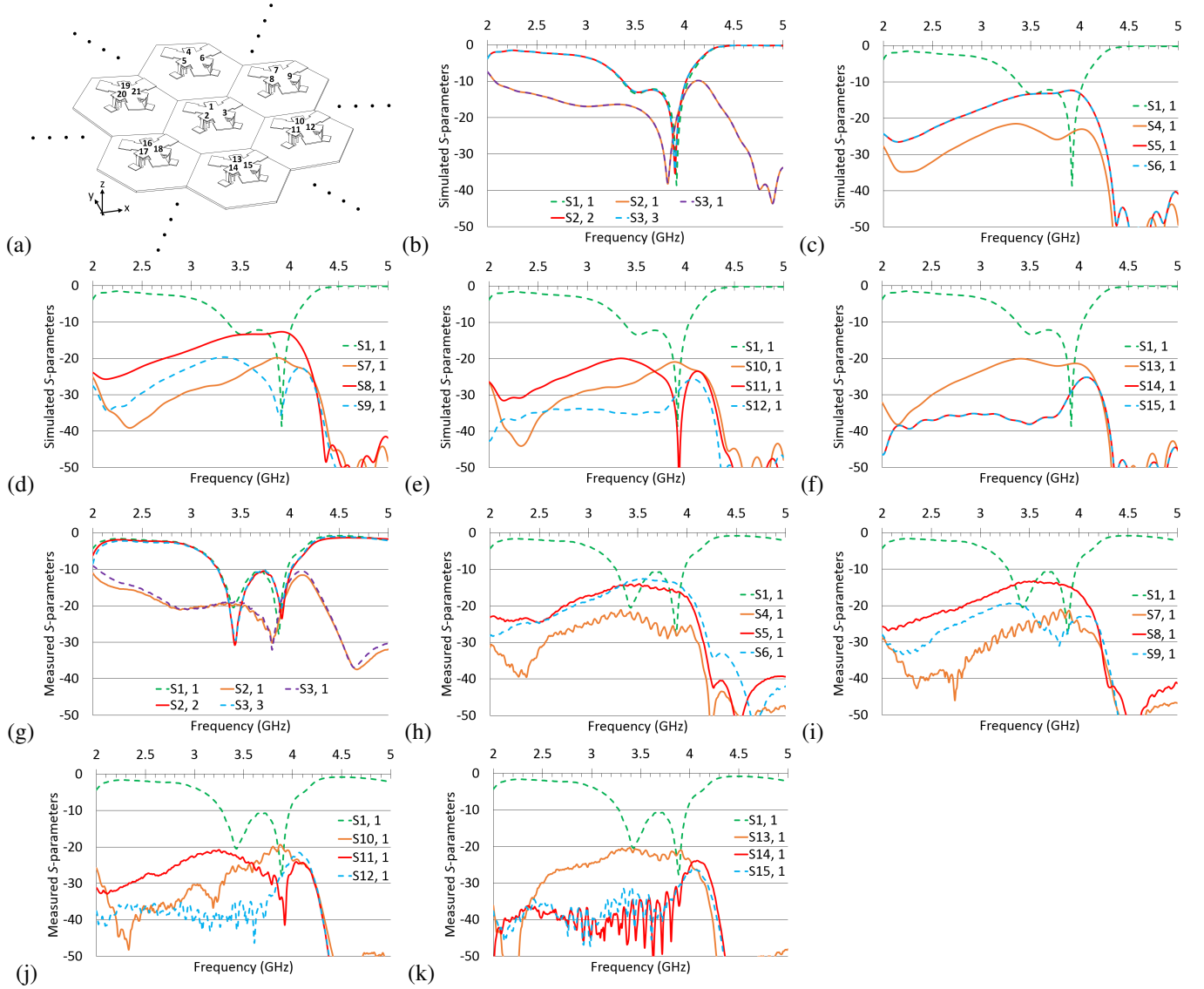
Fig. 11. Seven tessellated elements of wideband tri-port broadside antennas: (a) Geometry; (b)-(f) simulated S-parameters; and (g)-(k) measured S-parameters.

cells. Using the time-domain solver CST Microwave Studio [21], the simulated reflection coefficients of ports 1 to 3 and the simulated coupling coefficients with respect to port 1 are provided in Figs. 11(b)-(f). The corresponding measurement results are also given in Figs. 11(g)-(k). Compared to the single element configuration, the array element offers a similar 10 dB impedance bandwidth, ranging from 3.28 GHz to 3.97 GHz (BW = 19.0%) experimentally. In this particular example, the edge-to-edge and center-to-center element spacings are 23 mm and 60 mm, which correspond to $0.28\lambda_c$ and $0.72\lambda_c$ of unit cell element, respectively. It is noted that the element spacing of 60 mm was used in the narrowband version of tri-port broadside antenna array, with the center frequency of 3 GHz [5].

The close proximity of the array elements has a slight adverse effect on impedance matching. Since no special measure is adopted for suppressing the coupling between adjacent elements, ports 5, 6, 8 and 21 experience the largest coupling with respect to port 1, as they are closest to each other.

The rest of the coupling coefficients are mostly below -20 dB. Note that ports 16 to 18 and ports 19 to 21 can be thought as mirror images of ports 10 to 12 and ports 7 to 9, respectively. Therefore, their corresponding results are omitted for brevity. Furthermore, the simulated and measured radiation patterns of port 1 in this array setup are plotted in Fig. 12. As can be seen, the property of broadside radiation still holds within the operating bandwidth. However, due to coupling with adjacent elements and their ports, the maximum efficiency reduces to 71% in simulation. The approximately 20% efficiency drop is mainly attributed to the coupling loss with the four nearest ports (ports 5, 6, 8 and 21) of adjacent unit cells with average coupling coefficient of around -13 dB. Nevertheless, the antenna efficiency will not be significantly affected when more elements are tessellated on the periphery of the array. Furthermore, the backlobe radiations become smaller due to the big common ground plane in the array configuration. A further compression of the array size without incorporating any isolation technique is also possible. When
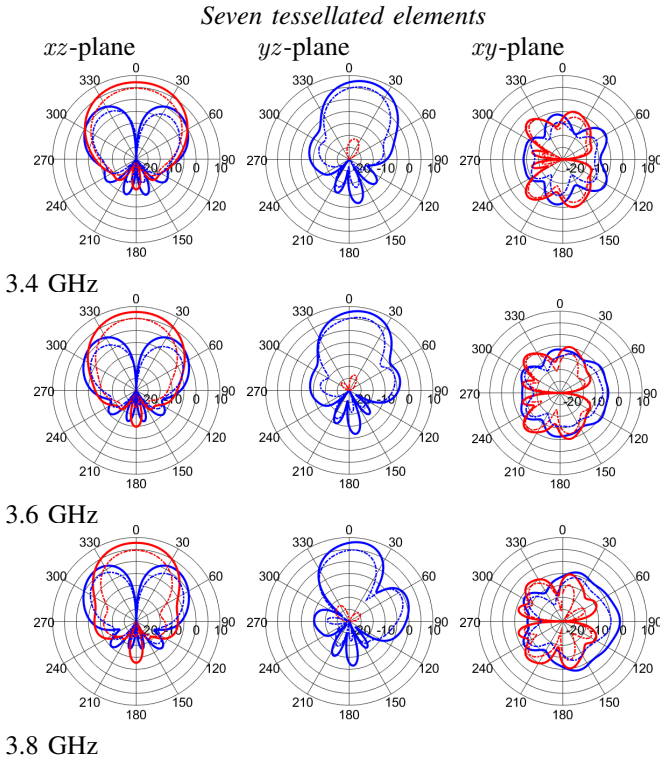
Seven tessellated elements

Fig. 12. Radiation patterns of seven tessellated elements of wideband tri-broadside radiation antennas obtained at port 1 with simulation (solid), measurement (dash-dot), E-phi (red), and E-theta (blue).

the center-to-center element spacing is compressed by a factor of 0.9 or 0.8 for instance, the worst mutual coupling between ports become -11.1 dB and -10.6 dB, respectively.

VI. CONCLUSION

In this paper, a bandwidth enhancement technique for tri-modal patch antennas is proposed. The key idea of the technique is to create two connected Y-shaped structures, from the original structure, each with a slightly different resonant frequency, but with similar radiation performance, to provide wideband operation. The working principle of the technique was analyzed with CMA. Six characteristic modes were utilized and divided into two groups corresponding to the two resonances of the Y-shaped structures. Feed design of the antenna was also achieved using CMA. To validate the design concept, a prototype was fabricated and tested. It is shown that the proposed bandwidth enhancement technique does not sacrifice the desirable properties of its base design, including compactness, multi-port, broadside radiation, low mutual coupling and rotational symmetry. Therefore, the proposed wideband tri-port antenna is suitable for constructing practical massive MIMO arrays.

ACKNOWLEDGMENT

REFERENCES

[1] E. G. Larsson, O. Edfors, F. Tufvesson, and T. L. Marzetta, "Massive MIMO for next generation wireless systems," *IEEE Commun. Mag.*, vol. 52, no. 2, pp. 186–195, 2014.

[2] L. Lu, G. Y. Li, A. L. Swindlehurst, A. Ashikhmin, and R. Zhang, "An overview of massive MIMO: Benefits and challenges," *IEEE J. Sel. Topics in Signal Process.*, vol. 8, no. 5, pp. 742–758, Aug., 2014.

[3] C. Y. Chiu and R. Murch, "Compact integrated three-broadside-mode patch antenna," *U.S. Patent Application 16/220,916*, filed Dec. 14, 2018.

[4] K. L. Wong, C. M. Chou, Y. J. Yang, and K. Y. Wang, "Multipolarized wideband circular patch antenna for fifth-generation multi-input-multi-output access-point application," *IEEE Antennas Wireless Propag. Lett.*, vol. 18, pp. 2184–2188, 2019.

[5] C. Y. Chiu, S. Shen, B. K. Lau, and R. Murch, "Design of a tri-modal broadside antenna element for compact massive MIMO arrays," *IEEE Antennas Propag. Mag. (accepted in 2019)*, in press. Available: https://ieeexplore.ieee.org/document/8946874.

[6] S. C. Ko and R. Murch, "Compact integrated diversity antenna for wireless communications," *IEEE Trans. Antennas Propag.*, vol. 49, no. 6, pp. 954–960, 2001.

[7] R. Garbacz and R. Turpin, "A generalized expansion for radiated and scattered fields," *IEEE Trans. Antennas Propag.*, vol. 19, no. 3, pp. 348–358, 1971.

[8] R. Harrington, "Theory of characteristic modes for conducting bodies," *IEEE Trans. Antennas Propag.*, vol. 19, no. 5, pp. 622–628, 1971.

[9] K. L. Wong, H. J. Chang, J. Z. Chen, and K. Y. Wang, "Three wideband monopolar patch antennas in a Y-shape structure for 5G multi-input-multi-output access points," *IEEE Antennas Wireless Propag. Lett.*, vol. 19, pp. 393–397, 2020.

[10] E. Rajo-Iglesias, O. Quevedo-Teruel, and M. Sánchez-Fernández, "Compact multimode patch antennas for MIMO applications," *IEEE Antennas Propag. Mag.*, vol. 50, no. 2, pp. 197–205, 2008.

[11] C. Y. Chiu, J. B. Yan, R. Murch, J. X. Yun, and R. G. Vaughan, "Design and implementation of a compact 6-port antenna," *IEEE Antennas Wireless Propag. Lett.*, vol. 8, pp. 767–770, 2009.

[12] D. Manteuffel and R. Martens, "Compact multimode multielement antenna for indoor UWB massive MIMO," *IEEE Trans. Antennas Propag.*, vol. 64, no. 7, pp. 2689–2697, 2016.

[13] T. Huynh and K. F. Lee, "Single-layer single-patch wideband microstrip antenna," *IET Electron. Lett.*, vol. 31, no. 16, pp. 1310–1312, 1995.

[14] K. L. Wong and W. H. Hsu, "Broadband triangular microstrip antenna with U-shaped slot," *IET Electron. Lett.*, vol. 33, no. 25, pp. 2085–2087, 1997.

[15] C. Wood, "Improved bandwidth of microstrip antennas using parasitic elements," *IEE Proc. H (Microw., Optics and Antennas)*, vol. 127, no. 4, pp. 231–234, 1980.

[16] K. Araki, H. Ueda, and T. Masayuki, "Numerical analysis of circular disk microstrip antennas with parasitic elements," *IEEE Trans. Antennas Propag.*, vol. 34, no. 12, pp. 1390–1394, 1986.

[17] Z. Miers, H. Li, and B. K. Lau, "Design of bandwidth-enhanced and multiband MIMO antennas using characteristic modes," *IEEE Antennas Wireless Propag. Lett.*, vol. 12, pp. 1696–1699, 2013.

[18] C. Deng, Z. Feng, and S. V. Hum, "MIMO mobile handset antenna merging characteristic modes for increased bandwidth," *IEEE Trans. Antennas Propag.*, vol. 64, no. 7, pp. 2660–2667, 2016.

[19] FEKO 14.0, Altair Engineering Inc., 2018.

[20] Z. Miers and B. K. Lau, "Wide band characteristic mode tracking utilizing far-field patterns," *IEEE Antennas Wireless Propag. Lett.*, vol. 14, pp. 1658–1661, 2015.

[21] CST Microwave Studio, CST Studio Suite TM, 2019.

[22] K. A. Obeidat, B. D. Raines, and R. G. Rojas, "Application of characteristic modes and non-foster multiport loading to the design of broadband antennas," *IEEE Trans. Antennas Propag.*, vol. 58, no. 1, pp. 203–207, 2010.

[23] F. Jiang, C. Y. Chiu, S. Shen, Q. Cheng, and R. Murch, "Pixel antenna optimization using N-port characteristic mode analysis," *IEEE Trans. Antennas Propag.*, vol. 68, no. 5, pp. 3336–3347, 2020.

[24] H. Jaafar, S. Collardey, and A. Sharaiha, "Optimized manipulation of the network characteristic modes for wideband small antenna matching," *IEEE Trans. Antennas Propag.*, vol. 65, no. 11, pp. 5757–5767, 2017.